

Short Communication

## Influence of (3-mercaptopropyl) methyldimethoxysilane on a GO/Zn coating and its corrosion resistance

Meng Ding, Xixun Shen\*

Shanghai Key Laboratory of Materials Protection and Advanced Materials in Electric Power, Shanghai Engineering Research Center of Heat-exchange System and Energy Saving, College of Environmental and Chemical Engineering, Shanghai University of Electric Power, Shanghai 200090, China

\*E-mail: [shenxixun@shiep.edu.cn](mailto:shenxixun@shiep.edu.cn)

Received: 1 May 2022 / Accepted: 10 June 2022 / Published: 4 July 2022

---

A GO/MPTS coating on a Zn coating electrodeposited on carbon steel was prepared by immersing zinc samples into suspension of graphene oxide/(3-mercaptopropyl) methyldimethoxysilane GM and then drying at 80°C. The silanol groups reacted with oxygen-containing functional groups on the GO during the hydrolysis process, and the GO was stacked layer by layer to construct a dense organic coating over the etched zinc surface. The synthesized GM coatings were characterized by FTIR, XRD, Raman spectroscopy and SEM. The corrosion behaviour of the galvanized carbon steel (GCS) and GCS coated with a GM composite coating exposed to a 3.5% NaCl solution were studied by potentiodynamic polarization and EIS. The results confirm that the GM coating can effectively protect GCS. Combined with the physical characterization of the GM-coated GCS explains its markedly increased corrosion resistance.

---

**Keywords:** Zn coating; (3-mercaptopropyl) methyldimethoxysilane; corrosion resistance; GO; galvanized carbon steel

### 1. INTRODUCTION

A zinc coating can be used as a sacrificial anode to protect a cathode, because zinc is more susceptible to corrosion than steel. However, the zinc coating also has some disadvantages, such relatively insufficient protection performance when dealing with the increasingly harsh natural environment. To develop zinc coatings isolated from corrosive media, many researchers have tried new methods. For example, chromate passivation is a typical process to improve the corrosion resistance of zinc coatings with simple operation, low cost and good film adhesion. Unfortunately, hexavalent chromium ions are very harmful to the environment. To protect the living environment and delay the corrosion of zinc coating, an extra organic or inorganic coating over the Zn coating can further improve the corrosion resistance.

It has been reported that organic and inorganic coatings, including rare earth conversion films[1, 2], silane films[3], conductive polymer films[4] and self-assembled films[5], can enhance the corrosion resistance of zinc coatings to some extent. Recent studies have shown that graphene oxide (GO), a two-dimensional nanofiller composed of  $sp^2$  hybrid carbon atoms, can significantly improve the anticorrosion ability of metals by extending the diffusion path of corrosive agents and reducing the porosity of the coating. For example, Rekha et al.[6] successfully prepared zinc-GO composite coatings by electrodeposition. Compared with that of the base zinc samples, the polarization resistance of zinc-GO samples increased significantly, and the corrosion rate decreased. Park et al.[7] directly deposited a GO-water suspension on the surface of carbon steel by electrophoresis to prepare a protective coating. However, the adhesion between this graphene film and the substrate was relatively weak, and it was difficult to provide sufficient protection for the steel because it does not form a sufficiently dense film. Parhizkar et al.[8] prepared 3-aminopropyl triethoxysilane-covalently modified GO films on a steel surface. The results show that the silane-modified GO film effectively improved the anticorrosion performance and decrease the cathodic delamination rate of the coating by inhibiting the penetration of the corrosive medium.

To ensure the effective dispersion of GO in metals and enhance the interfacial bonding between GO and metals, surface modified GO is usually chosen, which is an effective method to prevent the agglomeration of GO and enhance the anticorrosion ability of the coating. GO nanosheets contain a large number of epoxy functional groups, i.e., hydroxyl and carboxyl groups, providing sites for covalent functionalization[9]. Alkoxy groups in silane molecules are easy to hydrolyse in a water dispersion system to form silanol groups, which can condense with hydroxyl groups on the metal surface and silanol groups on adjacent silane molecules[10]. Therefore, the modification of GO with silane is a promising approach to improve the properties of composites. The alkoxy silane coupling agent groups react with the oxygen-containing groups of GO, and then undergo dehydration condensation with the hydroxyl groups on the metal matrix, thereby forming a dense protective film on metal surface.

Based on the above analysis, in this work, a GM composite coating was successfully prepared on galvanized carbon steel (GCS), denoted as the G-GM composite coating. The GCS sample prepared by the electrodeposition method was immersed in suspension of GO covalently modified with (3-mercaptopropyl)methyldimethoxysilane (MPTS), and the gel film was deposited on the surface of the GCS. After curing, a uniform and continuous composite coating with good anticorrosion performance was obtained on the surface of GCS. The micromorphology, chemical composition, and crystal structure of the GM composite coatings were systematically analysed. The electrochemical properties of the GCS and G-GM samples were also studied and their corrosion resistance mechanism was discussed.

## 2. EXPERIMENTAL

### 2.1 Preparation of GSC

To synthesis the graphene oxide (GO), the potassium permanganate, hydrogen peroxide (30%), phosphorus pentoxide and the graphite powder were purchased from Aladdin Reagents (Shanghai,

China). Other materials i.e sulphuric acid (98%) and potassium persulfate were purchased from Titan Technology Co., Ltd. (Shanghai, China). (3-mercaptopropyl)methyldimethoxysilane (MPTS), nitric acid, sodium hydroxide, glacial acetic acid, and anhydrous ethanol were purchased from Sinopharm Chemical Reagent Co., Ltd. (China). The chemicals used in the experiments were analytical grade.

The Zn coating was deposited on a 2 cm × 2 cm × 0.2 cm mild steel plate (Q235) in zinc electroplating bath with current density of 7 A/dm<sup>2</sup> and temperature of 30°C for 5 min. The composition of the zinc chloride-based electroplating solution can be found in the literature[11]. Subsequently, the galvanized carbon steel (GSC) sample prepared by electrodeposition was etched in 10% HNO<sub>3</sub> solution to obtain a uniform rough structure.

## 2.2 Preparation of the G-GM composite coating

GO was prepared by the Hummer method[12], and GO(0.1 g) nanosheets were dispersed in 50 ml of deionized water and then treated with ultrasonication for 2 h. A GO suspension was obtained by adding ethanol (150 ml) to the mixture and stirring vigorously for 2 h. The graphene oxide/(3-mercaptopropyl)methyldimethoxysilane (GO/MPTS) suspension was obtained when MPTS (1 ml) was added dropwise to the GO suspension, and the pH value of the suspension was adjusted to 4 with glacial acetic acid. To hydroxylate the surface of the etched GSC, the sample was immersed in a 20% NaOH solution for 5 minutes. For comparison, the hydroxylated GSCs were immersed in the above two suspensions (GO suspension and GO/MPTS suspension) for 30 min to prepare different films on the surface of the GSCs. Then, the samples were removed and placed into an oven at 80°C for curing. After cooling to room temperature, the samples were reimmersed in the above two suspensions (GO suspension and GO/MPTS suspension) for 30 minutes. After repeating this operation three times, the GSC-GO (G-G) composite coating, and the GSC-GO/MPTS (G-GM) composite coating were obtained.

## 2.3 Characterization

To analyse the functional groups present in substances, an infrared spectrum was obtained by means of a Spectrum Two Fourier transform infrared spectrometer, and the scanning range was 400-4000 cm<sup>-1</sup>. To analyse the defect degree of the material structure, Raman spectra over the wavenumber range of 300-3000 cm<sup>-1</sup> were obtained by means of a Dilor Labram-1B multichannel confocal microspectrometer, and the emission wavelength and the power were approximately 514 nm and 20 mV, respectively. To analyse the phase composition of the sample, X-ray diffraction (XRD) patterns were obtained on a Bruker D8 Advance X-ray diffractometer with Cu K $\alpha$  radiation and analysed by means of Jade software. The morphology of the GSC and G-GM composite coatings was analysed by means of a Japanese JSM-7800F field emission scanning electron microscope (SEM). The acceleration voltage used in the test was 5-20 kV. In addition, the elements contained in the composite coating were analysed and determined by using an attached energy spectrometer.

Electrochemical impedance spectroscopy (EIS) and potentiodynamic polarization measurements of the GSC and G-GM composite coatings were performed on a Chenhua CHI660E electrochemical

workstation with a three-electrode system in a 3.5 % NaCl solution. Before the AC impedance test, an open-circuit potential test was carried out for 400 seconds to stabilize as the initial potential in the AC impedance test. The test frequency was 0.01 Hz to 100k Hz, the amplitude was 0.005 V, and the scanning rate was 0.005 V/s. In order to study the reliability of the GSC and G-GM composite coatings, samples were tested for a long time with 5% NaCl solution in a neutral salt spray machine. The pH value of the 5% NaCl solution is within 6.5-7.2, the test temperature is 35°C, and the sedimentation rate of salt spray is between 1.0-2.0 ml/80 cm·h.

### 3. RESULTS AND DISCUSSION

#### 3.1 Structure of the G-GM composite coating

XRD is usually used to analyse the phase composition of materials. Fig. 1(a) shows the XRD patterns of graphite and GO. The XRD peaks of GO and graphite are obviously different, and the diffraction peak of the (002) crystal plane of GO appears at  $2\theta=11^\circ$ , which demonstrates the successful synthesis of GO. The XRD pattern of GO is similar to that reported in the literature[13-15]. Fig. 1(b) shows the Raman spectra obtained for the graphite, GO, and GO/MPTS (GM) samples. The Raman spectra of the GO and GM samples show D and G bands located at approximately  $1328\text{ cm}^{-1}$  and  $1595\text{ cm}^{-1}$ , respectively. The other peaks at approximately  $2600\text{ cm}^{-1}$  correspond to the 2D band. Similar patterns were also observed by others[13, 14]. The structurally disordered or defective bands at the edges of GO are associated with the D bands[16]. The stretching motion of the in-plane bond formed by  $sp^2$  carbon atoms is related to the G band. The second-order D band is the 2D band, which corresponds to the vibration of two phonon lattices. Compared with the weak D band and narrow G band of natural graphite, there are two obvious peaks and a slight redshift in both the G band and D band in the spectra of the GO and GM samples, indicating that hydroxyl and carbonyl groups have been grafted onto the carbon skeleton[17, 18]. The degree of the disorder or order of the samples was evaluated by the intensity ratio of the D band and G band ( $I_D/I_G$ )[19]. The calculated  $I_D/I_G$  values for GO and GM are 1.15 and 1.59, respectively, indicating that GO was successfully functionalized by silanol groups[20, 21]. Fourier transform infrared (FTIR) spectroscopy was also used to further analyse the functional groups of GO and GM, and the results are shown in Fig. 1(c). Compared with the infrared absorption peaks of graphite, the characteristic infrared peaks of GO include more obvious O-H, C=O, and C-O absorption peaks near  $3198\text{ cm}^{-1}$ ,  $1608\text{ cm}^{-1}$ , and  $1177\text{ cm}^{-1}$  [22, 23]. The presence of these oxygen characteristic peaks indicates that GO was successfully synthesized from graphite powder by the Hummer method. For GM, the absorption peaks attributed to C-Si appeared near  $1260\text{ cm}^{-1}$  and  $1400\text{ cm}^{-1}$ , characteristic peaks of Si-O-Si and S-S appeared near  $1100\text{ cm}^{-1}$  and  $400\text{ cm}^{-1}$  respectively, and the stretching vibration of Si-C appeared near  $700\text{ cm}^{-1}$ . The presence of these characteristic peaks proves that the reaction of MPTS with GO is a silanylation reaction of the silanols to form Si-O-C. The electronegativity of sulfur in the sulfhydryl group is weaker than that of the oxygen atom; therefore, the activity of the hydroxyl hydrogen should be higher than that of sulfhydryl hydrogen. Hydroxy hydrogen more easily attacks the epoxy group, while the sulfhydryl reaction is slightly less favourable, so the sulfhydryl group in MPTS does

not undergo a ring-opening reaction with the epoxy group. MPTS and GO successfully formed siloxane network[18, 24]. XRD patterns was used to analyse the crystal structure of the GSC, G-G, and G-GM composite coating, and the results are shown in Fig. 1(d). The as-deposited pure Zn coating on GSC sample exhibited a typical hexagonal crystal structure with five diffraction peaks corresponding to the (002) ( $2\theta=36.04^\circ$ ), (100) ( $2\theta=38.40^\circ$ ), (101) ( $2\theta=43.24^\circ$ ), (102) ( $2\theta=54.15^\circ$ ), and (110) ( $2\theta=70.24^\circ$ ) crystal planes. For the G-G composite coating, in addition to these five characteristic peaks, an obvious steamed bread like diffraction peak also appeared at a diffraction angle of  $2\theta=10^\circ$ , which exactly corresponds to the characteristic peak of GO[25, 26]. Such characteristic peaks corresponding to GO also appear in the diffraction pattern of the G-GM sample. The XRD results show that the GM film was successfully prepared on the GSC. No peaks of any other phases were observed for the G-GM composite coating, indicating that the structure of the GM nanocomposites remained unchanged after covalent modification[27].

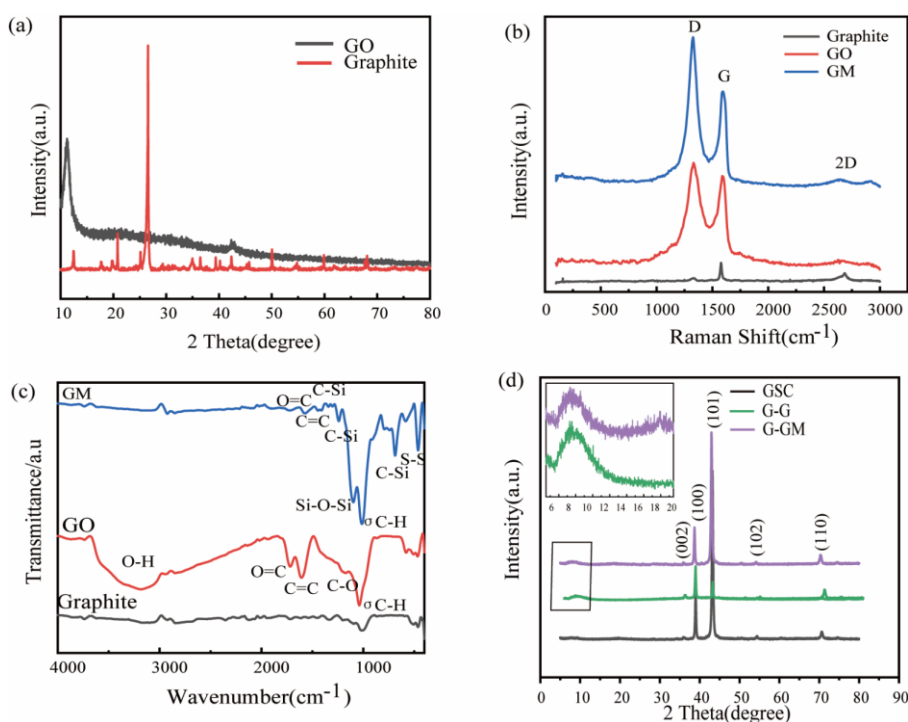


**Figure 1.** (a) XRD patterns of graphite and graphene oxide; (b) Raman spectra of graphite, GO and GM; (c) Infrared spectra of graphite, GO, GM; (d) XRD patterns of GSC, G-G and G-GM

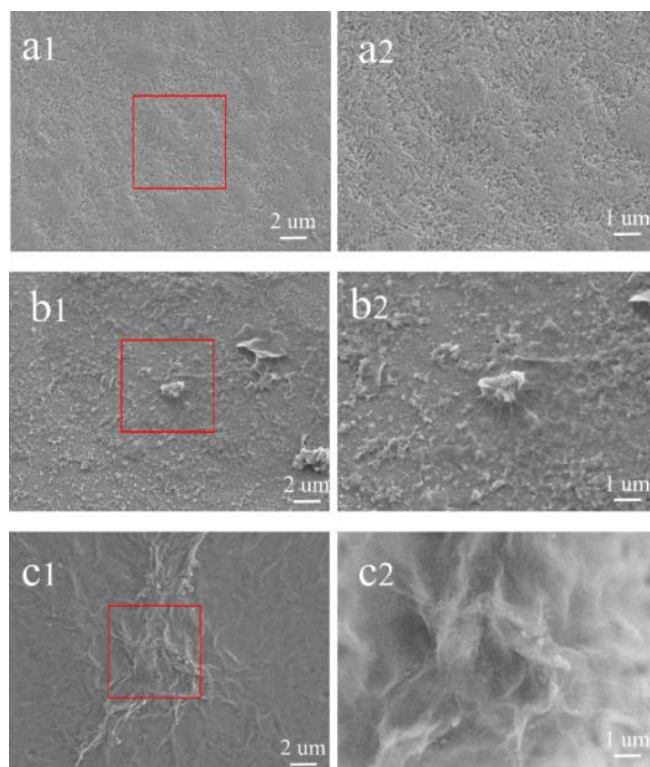
### 3.2 Surface morphology of the G-GM composite coating

Fig. 2 shows the SEM images of the GSC, G-G composite coating and G-GM composite coating. Fig. 2(a) shows the surface of GSC, which presents a staggered dendritic uplift and collapse structure. Fig. 2(b) shows the surface morphology of the G-G composite coating. The surface morphology of GSC was significantly changed after immersing the GSC samples in the GO suspension. As shown in Fig. 2(b), the staggered dendritic structure on the GSC surface disappears, and the surface shows a relatively

flat morphology with many irregular granular hills. In a magnified view of these hills, as shown in Fig. 2(b2), these granular hills show obvious fold characteristics, which is characteristic of GO aggregation[7, 26]. The morphological features observed in Fig. 2(b) show that simple graphene oxide is prone to agglomeration on the GSC. A certain portion is uniform, and some parts of the GO film are unaffected, which will make the corrosion resistance poor. Fig. 2(c) shows the surface morphology of the G-GM composite coating. The surface of the G-GM composite coating does not have an irregular hump structure, but the whole surface presents a typical fold structure, which means that the GO modified by MPTS can evenly cover the surface of the GSC. It can better provide a physical barrier for the surface of GSC to prevent the invasion of the corrosive medium, thereby improving the corrosion resistance of the composite material[7].

### 3.3 Chemical composition of the G-GM composite coating

To study the distribution of different elements in the composite coatings, the entire surface area of the G-GM sample shown in Fig. 2(c2) was analysed by SEM–EDS. The results are shown in Fig. 3, which shows that, Zn, C, O, Si, and S were detected on the surface of the G-GM sample, and the contents of each element are listed in Fig. 3(g). Fig. 3 shows that the distributions of Zn, C, O, Si and S were even in the detection area, which means that the GM film uniformly covered the surface of the GSC. The uniform composite coating further protected the GSC and prevented the intrusion of corrosive media, thereby improving the corrosion resistance.



**Figure 2.** SEM images of the surfaces a(1) and a(2) for the GSC; b(1) and b(2) for the G-G composite coating; c(1) and c(2) for the G-GM composite coating

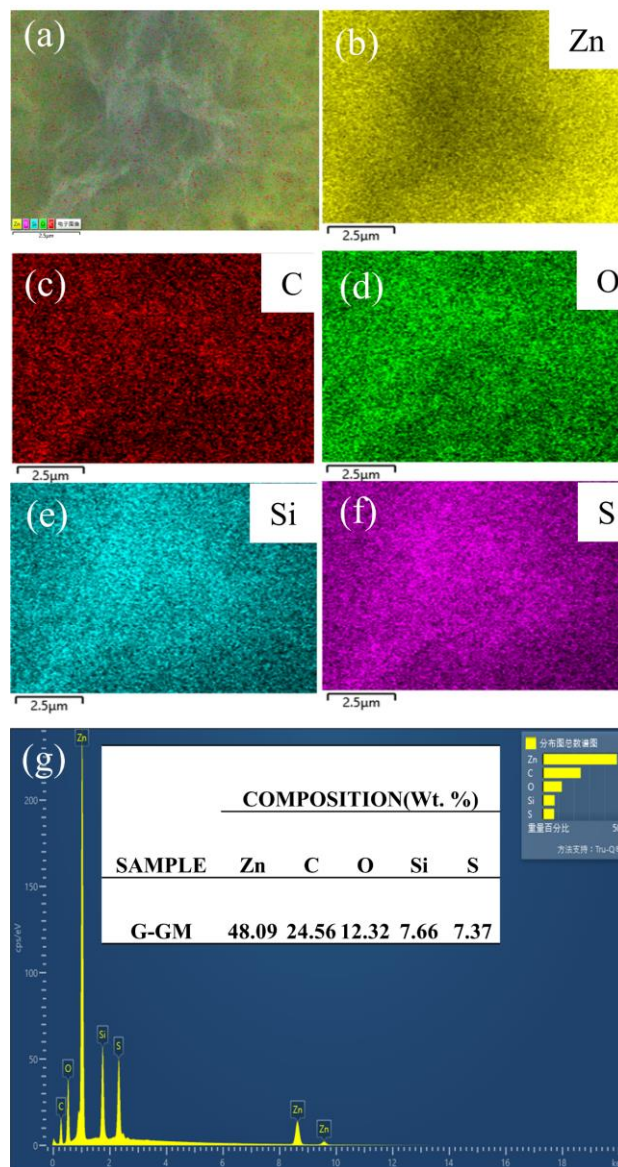


**Figure 3.** SEM images of (a) the G-GM composite coating; EDS mapping spectrum of (b) Zn, (c) C , (d) O, (e) Si, and (f) S; EDS analysis (wt %) of (g) the G-GM sample

### 3.4 Corrosion resistance of the G-GM composite coating

Electrochemical workstations were used to obtain the polarization plots of GSC and G-GM with a three-electrode system in 3.5% sodium chloride solution, and the test results are shown in Fig. 4. Fig. 4 shows that the GSC and G-GM samples exposed to 3.5% sodium chloride solution for 0 h and 72 h all exhibited similar anodic polarization behaviour with an obvious passivation process. A similar passivation region also appeared in the polarization plot of the G-G composite coating studied by Li et al[26, 28]. This phenomenon is common in zinc coatings and is caused by the adsorption of corrosion products on the coating surface[26]. For the GSC and G-GM composite coatings of 0 h exposure time, the anodic polarization process underwent plateau passivation before entering the severe anodic

corrosion stage[29]. Furthermore, upon preparation of the G-GM composite coating, the polarization plot position of the G-GM composite coating was significantly shifted, which indicated the anticorrosion ability of the coating had changed. Two important electrochemical parameters, corrosion potential ( $E_{corr}$ ) and corrosion current density ( $i_{corr}$ ), obtained from the polarization plot, as quantitative indicators to evaluate the corrosion resistance of the prepared materials. The values of these parameters density were extracted from the intercept of their Tafel slopes, and the results are listed in Table 1. According to Table 1, the  $e_{corr}$  value of the G-GM sample was approximately -1185 mV, which is 87 mV higher than that of GSC. The  $i_{corr}$  value of the G-GM sample was  $1.883 \times 10^{-6}$ , which is nearly two orders of magnitude smaller than that of GSC.

For the GSC and G-GM composite coatings of 72 h exposure time,  $e_{corr}$  value of the GSC (72 h) sample is was approximately about -1292 mV, which is 20 mV lower than that of the GSC (0 h). The  $i_{corr}$  value of the GSC (72 h) sample is was  $8.833 \times 10^{-4}$ , which is  $6.950 \times 10^{-4} \text{ A.cm}^{-2}$  higher than that of the GSC (0 h). And the  $i_{corr}$  value of the G-GM (72 h) sample is was  $4.836 \times 10^{-6}$ , which is  $2.718 \times 10^{-6} \text{ A.cm}^{-2}$  higher than that of the G-GM (0 h). A shift towards positive  $E_{corr}$  values and smaller  $i_{corr}$  values indicates improved corrosion resistance. After 72 hours immersion, the  $i_{corr}$  value of G-GM composite coating changed less than that of GSC coating. The above results indicate that the GM film can effectively reduce the corrosion rate of the zinc coating and can provide good protection for the GSC. The reason for improving the corrosion resistance of composite coatings after successful preparation of GM film on GSC is that it provides a physical barrier.

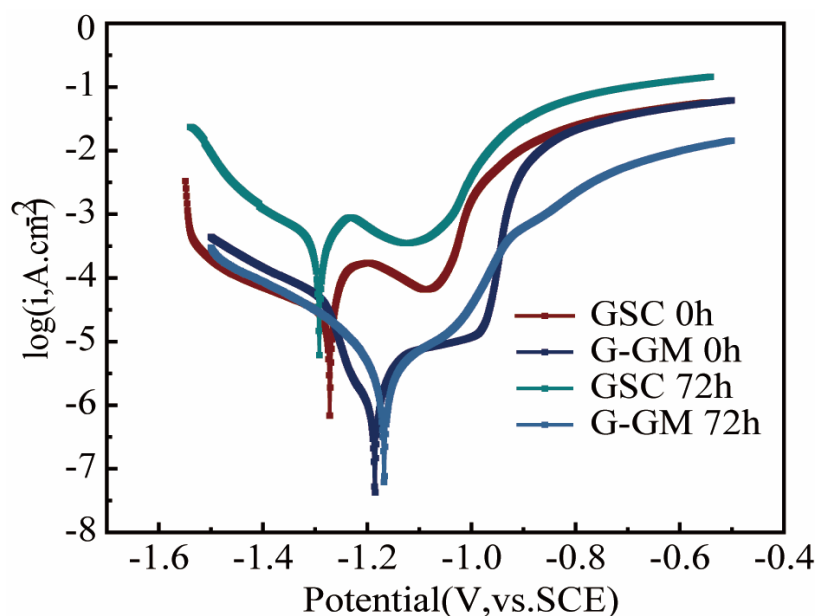


**Figure 4.** Polarization plots of the GSC and G-GM samples in a 3.5% sodium chloride solution at 0 h exposure time and 72 h exposure time

To study the electrochemical improvement mechanism of GM nanosheets on GSC in detail, electrochemical impedance spectroscopy (EIS) of the coatings was performed. Fig. 5 shows the electrochemical impedance diagrams of the GSC and G-GM samples in a 3.5% NaCl solution, including

the Nyquist diagram and Bode diagram. The equivalent circuit model previously proposed by Kumar et al.[30] (Fig. 5(d)) was used to simulate the electrode/solution interface and fitted with the aid of Z-view software.

**Table 1.** Corrosion potential ( $E_{\text{corr}}$ ) and corrosion current density ( $i_{\text{corr}}$ ) of the GSC and G-GM composite coatings

| Sample    | corrosion current density( $\text{A}\cdot\text{cm}^{-2}$ ) | corrosion potential(mV) |
|-----------|--|-------------------------|
| GSC 0 h   | $1.883 \cdot 10^{-4}$                                      | -1272                   |
| G-GM 0 h  | $2.118 \cdot 10^{-6}$                                      | -1185                   |
| GSC 72 h  | $8.833 \cdot 10^{-4}$                                      | -1292                   |
| G-GM 72 h | $4.836 \cdot 10^{-6}$                                      | -1168                   |

The fitting data extracted from the equivalent circuit are summarized in Table 2, corresponding to exposure to the 3.5% NaCl solution for 0 hours. Fig. 5(d) shows the equivalent circuit, where  $R_s$ ,  $R_{\text{coat}}$ , and  $R_{\text{ct}}$  represent the solution, coating and charge transfer resistance, respectively. The constant phase element of CPE is used to replace the capacitance element, and represents the nonuniform distribution of current and potential caused by the contribution of electrode porosity, surface roughness and coating composition. In Table 2, a value of the frequency dispersion factor 'n' greater than 0.9 indicates almost ideal capacitance behaviour. A lower 'n' value as observed for the coating ( $n < 0.5$ ) usually corresponds to a high roughness surface and indicates that the location where the oxidation–reduction reaction occurs is not uniform. Furthermore, a value of n between 0.5 and 0.8 indicates an uneven charge distribution on the electrode surface, which may be attributed to the ultrafine grain size and greater surface roughness resulting in a large grain boundary area[31]. Fig. 5(a) shows that the semicircle diameter of the Nyquist plots of the G-GM sample was larger than that of the GSC, which indicates a higher corrosion resistance performance of the G-GM samples[32]. The polarization resistance ( $R_p$ ) is an important parameter for evaluating the corrosion resistance of materials, and is the combined effect of the coating resistance ( $R_{\text{coat}}$ ) and the charge transfer resistance ( $R_{\text{ct}}$ ) referred to as the total polarization resistance ( $R_p = R_{\text{coat}} + R_{\text{ct}}$ )[32, 33].  $R_p$  is inversely proportional to the charge transfer rate; that is, the larger the polarization resistance is, the slower the corrosion rate. The  $R_s$  value is determined by the conductivity of the 3.5% NaCl solution. As seen from Table 2, the polarization resistance value of the G-GM composite coatings was larger than that of GSC, which is consistent with the results of the abovementioned polarization plot and the impedance radius.

It has been reported that the phase angle( $-\theta$ ) at high frequencies can be used to assess the integrity of coatings immersed in the electrochemical test solution[34]. Fig. 5(b) shows that the increase in the phase angle in the high-frequency range increased with the successful preparation of GM films on etchedGSC. It This shows that GO/MPTS GM films can improved the compactness and reduced the defects of the GSC surface. Compared with the Nyquist diagram, the impedance value  $|Z|$  also has the

same change trend. The low-frequency impedance modulus ( $|Z|$ ) is also often used as a parameter to evaluate the overall corrosion protection performance of coatings[35]. Compared with that of the GSC samples, the  $|Z|$  value of the G-GM composite coating was higher at low frequencies, which shows that the corrosion resistance of the G-GM samples was the best. Therefore, these results indicate that GM films can effectively improve the resistance of GSCs.

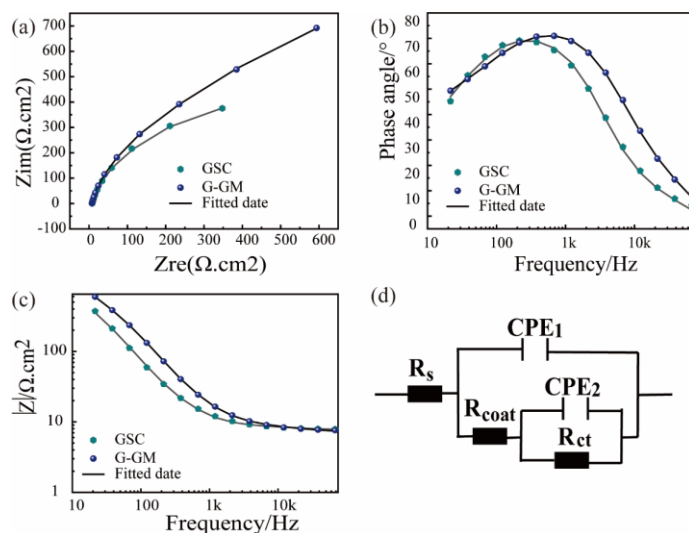


**Figure 5.** (a) Nyquist plot, (b) phase angle, and (c) Bode plot of GSC and the G-GM composite coating in a 3.5% sodium chloride solution

**Table 2.** Fitting parameters of the EIS data of GSC and G-GM composite coating in a 3.5% NaCl solution

| Samples | $R_s$<br>( $\Omega \cdot \text{cm}^2$ ) | $R_{\text{coat}}$<br>( $\Omega \cdot \text{cm}^2$ ) | $R_{\text{ct}}$<br>( $\Omega \cdot \text{cm}^2$ ) | CPE <sub>1</sub>        |       | CPE <sub>2</sub>        |       | $R_p$<br>( $\Omega \cdot \text{cm}^2$ ) |
|---------|---|---|---|-------------------------|-------|-------------------------|-------|---|
|         |   |   |   | $Y_1(W^{-1}cm^{-2}s^n)$ | $n_1$ | $Y_2(W^{-1}cm^{-2}s^n)$ | $n_2$ |   |
| GSC     | 7.903                                   | 635.5   | 448.3   | $1.473 \times 10^{-5}$  | 0.91  | $5.286 \times 10^{-5}$  | 0.76  | 1083.8                                  |
| G-GM    | 7.386                                   | 1009  | 1890  | $7.716 \times 10^{-6}$  | 0.89  | $2.331 \times 10^{-5}$  | 0.80  | 2899                                    |

In addition, Fig. 6 shows the results of the difference between the mass of the samples and that of the initial state, which was tested via the neutral salt spray (NSS) test during the 300 hours of the experiment. The change in the quality of the G-GM composite coating is always less than that of GSC within the 300 hours of the long-term experiment in the 5% NaCl salt fog test.

According to ISO 8407[36], the expression of the corrosion rate is as follows:

$$v = 10 \times m / (A \times \delta \times t) \tag{1}$$

where,  $m$  is the mass loss,  $A$  is the area exposed to corrosion,  $\delta$  is the material density, and  $t$  is the exposure time[37]. The calculated corrosion rates for the GSC and G-GM composite coatings were

8.629  $\mu\text{m}/\text{year}$  and 2.569  $\mu\text{m}/\text{year}$ , respectively. This indicates that the G-GM composite coating has stronger resistance to long-term corrosion than the GSC.

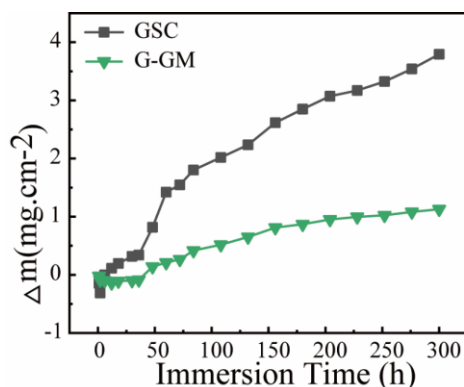


**Figure 6.** Mass change plot of different samples in the NSS experiment in a 5% NaCl solution

#### 4. CONCLUSIONS

In this paper, G-GM composite coating was prepared by immersion in a suspension of graphene oxide (GO) covalently modified with (3-mercaptopropyl)methyltrimethoxysilane (MPTS). After the dehydration condensation reaction of MPTS and GO, the typical fold structure of the GM coating was clearly observed on the composite coating. Electrochemical analysis showed that the G-GM composite coating has higher corrosion resistance than GSC. The corrosion potential and current density of the G-GM composite coating were approximately -1185 mV and  $1.883 \times 10^{-6}$ , respectively, which are nearly two orders of magnitude smaller than those of GSC. In addition, a neutral salt spray (NSS) test of the coatings exposed to a corrosive 5% NaCl solution for 300 h showed that the G-GM composite coatings exhibited better corrosion resistance than GSC. The above results indicate that the GM film can effectively reduce the corrosion rate of GSC and can provide a good protection for GSC.

#### ACKNOWLEDGMENT

This work was financially supported by the National Natural Science Foundation of China (No. 21972090); and the Science and Technology Commission of Shanghai Municipality (No.19DZ2271100).

#### References

1. P. Tianlan, M. Ruilin, *J. Rare Earths*, 27 (2009) 159-163.
2. Z. Yu, J. Hu, H. Meng, *Front. Mater.*, 7 (2020) 74.
3. J.K. Chang, C.S. Lin, W.J. Cheng, I.H. Lo, W.R. Wang, *Corros. Sci.*, 164 (2019) 108307.
4. H.N.T. Le, B. Garcia, C. Deslouis, Q.L. Xuan, *Electrochim. Acta*, 46 (2001) 4259-4272.
5. Y. Yamamoto, H. Nishihara, K. Aramaki, *J. Electrochem. Soc.*, 140 (1993) 436-443.

6. R.M. Y, C. Srivastava, *Corros. Sci.*, 152 (2019) 234-248.
7. J.H. Park, J.M. Park, *Surf. Coat. Technol.*, 254 (2014) 167-174.
8. N. Parhizkar, T. Shahrabi, B. Ramezanzadeh, *Corros. Sci.*, 123 (2017) 55-75.
9. Y.J. Wan, L.X. Gong, L.C. Tang, L.B. Wu, J.X. Jiang, *composites, Part A*, 64 (2014), 79-89.
10. Y. Dun, Y. Zuo, *Appl. Surf. Sci.*, 416 (2017) 492-502.
11. J. Sheng, X. Shen, Y. Wang, Q. Xu, X. Zhang, *Mater. Corros.*, 70 (2019) 1044-1055.
12. W.S. Hummers, J.R, R.E. Offeman, *J. Am. Chem. Soc.*, 80 (1958) 1339-1339.
13. N. Sharma, V. Jain, M. Kumari, R. Gupta, S.K. Sharma, K.Sachdev, *Macromol. Symp.*, 376 (2017) 1700006.
14. W.Li, B. Zhou, M. Wang, Z. Li, R. Ren, *J. Mater. Sci.*, 50 (2015) 5402-5410.
15. D.C. Marcano, D.V. Kosynkin, J.M. Berlin, A. Sinitskii, Z. Sun, A. Slersarev, L.B. Alemany, W. Lu, J.M. Tour, *ACS Nano*, 4 (2010) 4806-4814.
16. D. Kostiuik, M. Bodik, P. Siffalovic, M. Jergel, Y. Halahovets, M. Hodas, M. Pelletta, M. Pelach, M. Hulman, Z. Spitalsky, M. Omastova, E. Majkova, *J. Raman Spectrosc.*, 47 (2016) 391.
17. H. Cen, Z. Chen, *Colloids Surf., A*, 615 (2021) 126216.
18. M.D. Sousa, C.H.Z. Martins, L.S.Franqui, MD, L.C. Fonseca, F.S. Delite, E.M. Lanzoli, D.S.T. Martinez, O.L.Alves, *J. Mater. Chem. B*, 6 (2018) 2803-2812.
19. Y. Chen, C. Zhao, Z. Wang, H. Zhang, S. Wen, J. Song, *Proc. SPIE Int. Opt.Eng.*, 51 (2012) 084203.
20. J. Yan, Z. Fan, T. Wei, W. Qian, M. Zhang, F. Wei, *Carbon*, 48 (2010) 3825-3833.
21. C. Chen, M. Long, M. Xia, C. Zhang, W. Cai, *Nanoscale Res. Lett.*, 7 (2012) 1-5.
22. J. Chen, B. Yao, C. Li, G. Shi, *Carbon*, 64 (2013) 225-229.
23. X. Wang, W. Xing, P. Zhang, L. Song, H. Yang, Y. Hu, *Compos. Sci. Technol.* 72 (2012) 737-743.
24. C. Zhang, J. Sui, J. Li, Y. Tang, W. Cai, *Chem. Eng. J.*, 210 (2012) 45-52.
25. Z. Zhen, S. Wang, L. Lan, Y. Zhang, Y. Zhang, *Compos. Sci. Technol.*, 68 (2008) 1727-1733.
26. R. Li, J. Liang, Y. Hou, Q. Chu, *RSC Adv.*, 5 (2015) 60698-60707.
27. C. Zhang, J. Sui, J. Li, Y. Tang, W. Cai, *Chem. Eng. J.*, 210 (2012) 45-52.
28. B. Yang, P. Zhang, G. Wang, A. Wang, X. Chen, S. Wei, J. Xie, *Coatings*, 9 (2019) 758
29. M. Mirak, M. Alizadeh, M.N. Ashtiani, M. Ghaffaric, *J. Mech. Behav. Biomed. Mater.*, 62 (2016) 282-290.
30. M.P. Kumar, M.P. Singh, C. Srivastava, *RSC Adv.*, 5 (2015) 25603-25608.
31. S. Arora, C. Srivastava, *Metall. Mater. Trans. A*, 51 (2020) 4274-4287.
32. A. Aliyu, C. Srivastava, *J. Alloys Compd.*, 864 (2021) 158851.
33. X. Shen, J. Sheng, Q. Zhang, Q. Xu, D. Cheng, *J. Mater. Eng. Perform.*, 27 (2018) 3750-3761.
34. Y. Xie, M. Chen, D. Xie, L. Zhong, X. Zhang, *Corros. Sci.*, 128 (2017) 1-8.
35. B. Xue, M. Yu, J. Liu, S. Li, L. Xiong, X. Kong, *J. Electrochem. Soc.*, 163 (2016) C798-C806.
36. K.E. García, A.L. Morales, C.A. Barrero, J.M. Greneche, *Corros. Sci.*, 48 (2006) 2813-2830.
37. A.L. Morales, D. Cartagena, J.L. Rendon, A. Valencia, *Phys. Status Solidi B*, 220 (2000) 351-356.